J. Fluid Mech. (2001), *vol.* 435, *pp.* 351–376. Printed in the United Kingdom

Evaporation and combustion of thin films of liquid fuels

By J. ARMENDÁRIZ† AND M. MATALON

Engineering Sciences and Applied Mathematics, McCormick School of Engineering and Applied Science, Northwestern University, Evanston, IL 60208-3125, USA

(Received 10 April 2000 and in revised form 20 October 2000)

We consider the evaporation and subsequent burning of thin films of liquid fuels. Previous studies on liquid films, with and without evaporation, have primarily considered the gas phase to be passive. The new element in this study is the introduction of combustion and the examination of both the liquid and gas phases and their effect on the film's behaviour. For the case of a liquid film burning in quiescent air we show that the problem can be simplified to a single nonlinear evolution equation for the film thickness. All remaining variables, which are simply expressed in terms of the function describing the instantaneous position of the liquid–vapour interface, are subsequently determined. This equation is then solved in order to understand the dynamics of the film in the presence of evaporation and combustion.

The planar configuration is discussed first. Predictions for the total evaporation time are obtained, along with the time history of the film thickness, the interfacial surface temperature, the flame standoff distance and its temperature, and the mass burning rate. The dependence of the burning characteristics on the fuel and oxidizer Lewis numbers, which measure the relative importance of thermal and molecular diffusivities, is also determined. Second, we analyse the case of a non-planar interface, where temperature variations along the film's surface cause fluid motion in the liquid that could either dampen or amplify spatial non-uniformities. We show that, while thermocapillarity has the tendency to destabilize the planar interface, combustion acts to reduce this effect. In particular, when the heat release by combustion is substantial, all disturbances are obliterated, the film remains nearly planar and the burning occurs along nearly horizontal surfaces.

1. Introduction

Thin liquid films play a substantial role in various scientific areas such as biology, physics, chemistry and geology. In engineering applications, they serve as agents for heat and mass transport and are common in lubrication systems. Our interest stems from applications involving films of liquid fuels. An accidental spillage of a flammable fluid can be a fire hazard. A leak of liquid fuel at high pressure in industrial applications may produce a flow of burning liquid over solid surfaces, a situation referred to as a 'running liquid fire' in the petrochemical industries. In combustion devices where a liquid fuel jet is atomized into droplets, the development of thin liquid films flowing along the relatively colder walls is often possible. Understanding the burning characteristics of these films is essential for the overall control of the combustion efficiency.

† Present address: IMA, University of Minnesota, Minneapolis, MN 55455-0463, USA.

Over the past few decades much work has been done on the stability of thin liquid films with and without evaporation and in the presence of various effects such as surface tension, vapour recoil and molecular forces as well as with the presence of soluble and insoluble surface-active agents (cf. Oron, Davis & Bankoff 1997). A similar theoretical study which examines the combustion of thin films has not been done. This investigation provides a general formulation for such studies. Unlike most previous works where the gas-phase processes were considered passive, our formulation accounts for the interaction between the liquid and the gas and recognizes the fact that the dynamics could be profoundly influenced by interfacial effects.

The burning of liquid fuels is a complex phenomenon; it is an unsteady process, since as a result of vaporization the surface of the film recedes continually, and a process that exhibits a strong coupling between the liquid and gas phases. The fuel vapour produced as a result of evaporation can either burn as a 'pool fire', with nearly uniform horizontal surfaces, or as a flame spreading along the surface of the film (cf. Ross 1994). In this work we will be primarily concerned with a configuration that is relevant to pool fires and, in particular, with the case of a liquid film burning in quiescent air. Our formulation, however, is quite general, allowing for forced and natural convection with more far-reaching applications.

The fluid dynamics in the liquid phase is simplified by exploiting the disparity between the film thickness and the typically much larger transverse characteristic length. Another key simplification is the assumption of a small gas-to-liquid density ratio, a good approximation for most typical fuels. As a consequence, the film recedes relatively slowly and the gas-phase processes are quasi-steady. In this study the fast chemistry limit has also been considered with the burning occurring along a thin diffusion flame located where the fuel vapour meets the oxidizer at stoichiometric proportions. Incomplete combustion, including the possibility of extinction, could be easily incorporated using more general jump relationships across the diffusion flame surface (Cheatham & Matalon 2000). With these simplifications the problem is systematically reduced to what amounts to boundary layer equations in the gas phase and the lubrication approximation in the liquid phase. For the case of a liquid film burning in quiescent air, the problem is further simplified to a single nonlinear evolution equation that describes the local and instantaneous thickness of the film. All remaining variables, which are simply expressed in terms of the function describing the instantaneous position of the liquid–vapour interface, are subsequently determined. Similarly to previous studies (Williams & Davis 1982; Burelbach, Bankoff & Davis 1988; Krishnamoorthy, Ramaswamy & Joo 1995; Oron *et al.* 1997) this equation accounts for gravity and thermocapillary effects. However, it also depends on the local surface temperature and on the mass flux leaving the surface of the film, two quantities that are determined by the details of the gas-phase processes.

There are only few combustion-related studies that have some relation to the present investigation. Sirignano & Glassman (1970) considered the surface-tension-driven convective motion in a liquid pool and provided a solution that describes the local deformation of the free surface. They considered the uncoupled system, ignoring the gas-phase phenomena and the energy transfer from the gas to the liquid. Their analysis, which extends that of Landau & Lifshitz (1959, p. 236) by introducing a relative motion between the interface and the bottom surface of the pool, has been interpreted in the context of the flame spread problem. Aharon & Shaw (1996) carried out a linear stability analysis to determine the influence of thermal and solutal Marangoni effects on an evaporating droplet. By adopting a quasi-steady

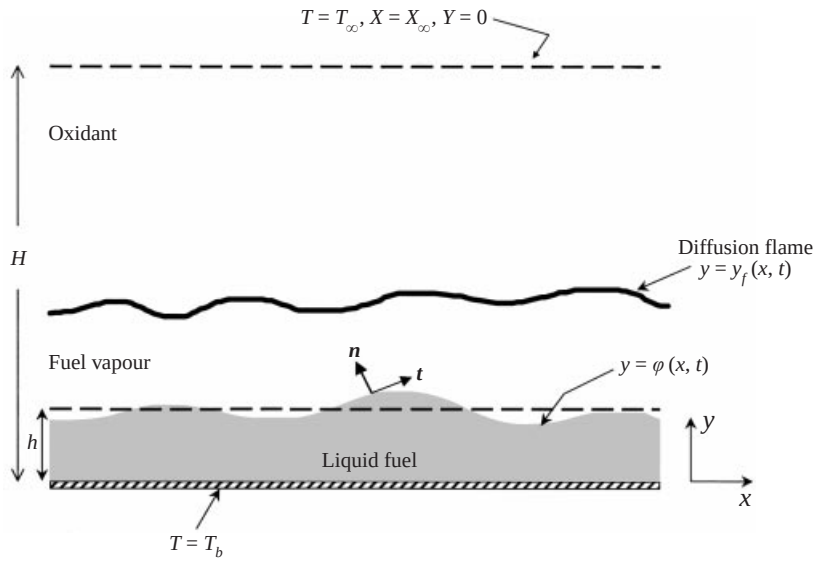

FIGURE 1. Configuration of the problem.

approximation while neglecting gravity and surface deformation, a critical droplet radius was identified above which an instability results. They concluded that, for the conditions considered, thermocapillary effects have a stabilizing influence. The correspondence of their finding to our results will be discussed later.

2. Formulation

A thin liquid layer lies on a solid surface located at $y = 0$ and is maintained at a uniform temperature T_b. The film is laterally unbounded and consists of a combustible, incompressible fluid of constant material properties. The liquid is evaporating at its surface and the fuel vapour thus formed is burning in the gas phase with the ambient oxidizer. The liquid–vapour interface is described by $y = \varphi(x, t)$ where x is the lateral coordinate and t is the time variable. Thus, unit normal and tangent vectors to the interface are respectively given by

$$\boldsymbol{n} = \frac{(-\partial\varphi/\partial x,\ 1)}{\sqrt{1 + (\partial\varphi/\partial x)^2}}, \quad \boldsymbol{t} = \frac{(1,\ \partial\varphi/\partial x)}{\sqrt{1 + (\partial\varphi/\partial x)^2}},$$

and the velocity of the interface along the normal is

$$V_I = \frac{\partial\varphi/\partial t}{\sqrt{1 + (\partial\varphi/\partial x)^2}}.$$

The chemical activity is modelled by an overall one-step chemical reaction of the form

$$\nu_F\ \text{Fuel} + \nu_X\ \text{oXidizer} \rightarrow \text{Products}$$

where ν_i is the stoichiometric coefficient of species i and the subscripts F, X stand for fuel and oxidizer, respectively. It is assumed that the fuel vapour burns to completion within a finite 'boundary layer' of thickness H. The configuration is shown in figure 1.

We denote the velocity field by $\boldsymbol{v}$, the temperature and density by T and ρ and the mass fractions of fuel and oxidizer by Y and X, respectively. The accent $\hat{}$ identifies

the variables in the liquid phase. Conservation of mass, momentum and energy in each of the two phases are:

liquid phase

$$\nabla \cdot \hat{\boldsymbol{v}} = 0, \tag{2.1}$$

$$\rho_\ell \frac{\mathrm{D}\hat{\boldsymbol{v}}}{Dt} = \nabla \cdot \hat{\Sigma} + \rho_\ell \boldsymbol{g}, \tag{2.2}$$

$$\rho_\ell c_{p_\ell} \frac{\mathrm{D}\hat{T}}{Dt} - \lambda_\ell \nabla^2 \hat{T} = 0; \tag{2.3}$$

gas phase

$$\frac{\partial \rho}{\partial t} + \nabla \cdot \rho \boldsymbol{v} = 0, \tag{2.4}$$

$$\rho \frac{\mathrm{D}\boldsymbol{v}}{Dt} = \nabla \cdot \Sigma + \rho \boldsymbol{g}, \tag{2.5}$$

$$\rho c_{p_g} \frac{\mathrm{D}T}{\mathrm{D}t} - \lambda_g \nabla^2 T = Q\omega, \tag{2.6}$$

$$\rho \frac{\mathrm{D}Y}{\mathrm{D}t} - \rho \mathscr{D}_F \nabla^2 Y = -\nu_F W_F \omega, \tag{2.7}$$

$$\rho \frac{\mathrm{D}X}{\mathrm{D}t} - \rho \mathscr{D}_X \nabla^2 X = -\nu_X W_X \omega. \tag{2.8}$$

In these equations $\mathrm{D}/\mathrm{D}t$ is the convective derivative, $\hat{\Sigma}$ and Σ are the stress tensors, given by $\hat{\Sigma} = -\hat{p}\boldsymbol{I} + \mu_\ell(\nabla\hat{\boldsymbol{v}} + \nabla\hat{\boldsymbol{v}}^{\mathrm{T}})$ in the liquid and $\Sigma = -p\boldsymbol{I} + \mu\{(\nabla\boldsymbol{v} + \nabla\boldsymbol{v}^{\mathrm{T}}) - \frac{2}{3}(\nabla\cdot\boldsymbol{v})\boldsymbol{I}\}$ in the gas with the superscript $^{\mathrm{T}}$ denoting the transpose, $\boldsymbol{I}$ a unit tensor and $\hat{p}$, p the pressure in the respective phases. The gravitational force (per unit mass) is denoted by $\boldsymbol{g}$ and is acting downwards, in the negative y-direction. The liquid density ρ_ℓ is taken as a constant, but the density of the gas ρ varies with temperature, as discussed below. The coefficients c_{p_ℓ} and λ_ℓ, which are both assumed constant, represent the specific heat and thermal conductivity of the liquid. The liquid viscosity μ_ℓ typically varies with temperature but, for simplicity, it will be treated here as a constant; the implication of this assumption will be further discussed in the conclusions. The specific heat and thermal conductivity of the gaseous mixture, c_{p_g} and λ_g, are also taken as constant but the viscosity μ may be allowed to vary with temperature. The molecular weight of species i is denoted by W_i and the molecular diffusivity $\mathscr{D}_i$ is assumed to vary with temperature such that $\rho\mathscr{D}_i$ is constant. The chemical reaction rate obeys the Arrhenius law

$$\omega = \mathscr{B}\left(\frac{\rho Y}{W_F}\right)\left(\frac{\rho X}{W_X}\right)\mathrm{e}^{-E/R^o T} \tag{2.9}$$

where $\mathscr{B}$ is a pre-exponential factor, E is the overall activation energy and R^o is the universal gas constant. The total chemical heat release is denoted by Q.

In writing these equations, the kinetic energy has been neglected, as was the rate of dissipation of mechanical energy due to shear viscosity. Since the characteristic gas-phase velocities are typically small compared to the speed of sound, the gas-phase processes are considered nearly isobaric, with $P \approx P_\infty$, the pressure in the ambient

gas. The equation of state thus reduces to

$$\rho T = \frac{\bar{W}}{R^o} P_\infty \tag{2.10}$$

with $\bar{W}$, the average molecular weight of the mixture, taken as constant. The pressure p appearing in Σ is the small pressure variation $P - P_\infty$, of the order of the square of the representative Mach number.

The boundary conditions are

$$\hat{\boldsymbol{v}} = 0, \quad \hat{T} = T_b \quad \text{at} \quad y = 0, \tag{2.11}$$

corresponding to the no-slip and isothermal conditions at the solid surface, and

$$T = T_\infty, \quad \rho = \rho_\infty, \quad X = X_\infty, \quad Y = 0 \quad \text{at} \quad y = H, \tag{2.12}$$

corresponding to the specified uniform state at the edge of the combustion layer. The velocity field at $y = H$ is also specified by the external flow.

At the interface, $y = \varphi(x, t)$, the vapour–liquid jump conditions are as follows: The overall mass balance is

$$\rho_\ell(\hat{\boldsymbol{v}} \cdot \boldsymbol{n} - V_I) = \rho(\boldsymbol{v} \cdot \boldsymbol{n} - V_I) \equiv m, \tag{2.13}$$

where m denotes the net mass flux across the interface. The mass balance for the fuel and oxidizer are

$$mY - \rho \mathscr{D}_F \frac{\partial Y}{\partial n} = mY_\ell, \tag{2.14}$$

$$mX - \rho \mathscr{D}_X \frac{\partial X}{\partial n} = 0, \tag{2.15}$$

where Y_ℓ is the fuel mass fraction in the liquid. The balance of normal stress is

$$m(\hat{\boldsymbol{v}} - \boldsymbol{v}) \cdot \boldsymbol{n} - \boldsymbol{n} \cdot (\hat{\Sigma} - \Sigma) \cdot \boldsymbol{n} = \sigma \nabla \cdot \boldsymbol{n}, \tag{2.16}$$

where $\nabla \cdot \boldsymbol{n}$ is twice the mean curvature and σ is the surface tension. The balance of shear stress is

$$m(\hat{\boldsymbol{v}} - \boldsymbol{v}) \cdot \boldsymbol{t} - \boldsymbol{t} \cdot (\hat{\Sigma} - \Sigma) \cdot \boldsymbol{n} = -\boldsymbol{t} \cdot \nabla \sigma. \tag{2.17}$$

The balance of energy is

$$\lambda_g \frac{\partial T}{\partial n} - \lambda_\ell \frac{\partial \hat{T}}{\partial n} = mL_\mathrm{v}, \tag{2.18}$$

where L_v is the latent heat of vaporization. Finally, no slip at the interface between the two fluids

$$(\hat{\boldsymbol{v}} - \boldsymbol{v}) \cdot \boldsymbol{t} = 0, \tag{2.19}$$

and continuity in temperature at the interface $T = \hat{T}$ must be applied.

The Clausius–Clapeyron condition that relates the partial pressure of the fuel vapour to the temperature in the vicinity of the interface is expressed as

$$\frac{Y P_\infty}{W_F / \bar{W}} = P^o \exp\left\{ -\frac{L_\mathrm{v}}{R^o / W_F} \left(\frac{1}{T} - \frac{1}{T_B} \right) \right\}, \tag{2.20}$$

where T_B is the boiling temperature evaluated at the reference pressure P^o. The surface tension σ is assumed to depend linearly on the temperature, namely

$$\sigma = \sigma_0 - \gamma(\hat{T} - T_\infty), \tag{2.21}$$

	Methanol	Ethanol	Hexane	Octane	Air
ρ_l [kg m^{-3}]	791	789	660	703	—
ρ_g [kg m^{-3}]	—	—	—	—	1.23
μ_l [kg m^{-1} s^{-1}]	0.6×10^{-3}	1.2×10^{-3}	0.3×10^{-3}	0.5×10^{-3}	—
μ_g [kg m^{-1} s^{-1}]	1.0×10^{-5}	0.9×10^{-5}	0.7×10^{-5}	0.5×10^{-5}	1.8×10^{-5}

TABLE 1. Density and viscosity of representative liquid fuels and air at 300 K.

where σ_0 is evaluated at the reference state $T = T_\infty$. For most common liquids, the gradient $\gamma = -\mathrm{d}\sigma/\mathrm{d}T > 0$.

3. Scaling and non-dimensionalization

A key simplification in scaling the governing equations is the assumption that transverse variations along the film occur on a much larger scale than the scale h that characterizes the film thickness. In other words, a long-wavelength approximation is adopted so that, if the vertical dimension is scaled with respect to the initial film thickness h, the horizontal coordinate is scaled with respect to h/ϵ, with the aspect ratio $\epsilon \ll 1$. The horizontal velocity component in the liquid phase is scaled using the ratio of the viscous diffusivity to the characteristic length, namely using $\mu_\ell \epsilon/\rho_\ell h$ as a unit. Time is non-dimensionalized accordingly, with respect to $\rho_\ell h^2/\mu_\ell \epsilon^2$. In scaling the horizontal velocity component in the gas phase we use the thermal diffusivity of the mixture $\mathscr{D}_{\mathrm{th}} = \lambda_g/\rho_g c_{p_g}$ instead of the viscous diffusivity, so that $\mathscr{D}_{\mathrm{th}}/h\epsilon$ is used as a unit. The characteristic density ρ_g was chosen as the density of the ambient gas, namely $\rho_g = \rho_\infty$. In order to conserve mass $\hat{v}/\hat{u}$ and v/u must both be $O(\epsilon)$ so that the vertical velocity components are scaled accordingly. Consistent with these choices, the net mass flux m leaving the surface of the film is made dimensionless with respect to λ_g/hc_{p_g}. The temperature is scaled with respect to the ambient temperature T_∞, and the characteristic viscosity is taken to be that of the ambient gas, namely $\mu_g = \mu_\infty$. The pressure in the liquid and gas phases is respectively referred to $\mu_\ell^2/\rho_\ell h^2$ and $\rho_g \mathscr{D}_{\mathrm{th}}^2/h^2\epsilon^2$. Finally, the fuel and oxidizer mass fractions are both scaled with respect to Y_{ℓ}.

Another key assumption used in the analysis is the realization that the gas-to-liquid density and viscosity ratios are small. Typical values for representative alcohol and hydrocarbon fuels are shown in table 1 and with the characteristic density and viscosity of the gaseous mixture ρ_g and μ_g determined mostly by the properties of air, we see that the ratios $\rho_g/\rho_\ell \approx 10^{-3}$ and $\mu_g/\mu_\ell \approx 10^{-2}$. We thus consider the distinguished limit $\rho_g/\rho_\ell = \epsilon^2$ and consequently write $\mu_g/\mu_\ell \sim \epsilon^2$, allowing here for an $O(1)$ proportionally constant. The ratio of thermal conductivities, λ_g/λ_ℓ is treated as $O(1)$.

We note that it may have been more appropriate to scale the equations using the evaporative time scale $\mathscr{D}_{\mathrm{th}}^{-1} h^2(\rho_\ell/\rho_g)$, which represents the time that it takes for a film of thickness h with a planar interface to evaporate completely (see § 5). It is, however, equivalent in magnitude to the viscous time scale we have chosen for non-dimensionalization, their ratio being

$$\alpha \equiv \frac{\mu_g/\rho_g}{\mu_\ell/\rho_\ell} Pr = O(1),$$

where $Pr = \mu_g c_{p_g}/\lambda_g$ is the gas-phase Prandtl number. The choice we have adopted was made so that the resulting evolution equation resembles in form those appearing in previous thin-film studies (cf. Oron *et al.* 1997).

The dimensionless governing equations and boundary conditions, after taking the limit $\epsilon \to 0$, become (the same symbols are used below for the dimensionless quantities as well):

liquid phase

$$\frac{\partial \hat{u}}{\partial x} + \frac{\partial \hat{v}}{\partial y} = 0, \tag{3.1}$$

$$\frac{\partial \hat{p}}{\partial y} + G = 0, \quad \frac{\partial \hat{p}}{\partial x} = \frac{\partial^2 \hat{u}}{\partial y^2}, \tag{3.2}$$

$$\frac{\partial^2 \hat{T}}{\partial y^2} = 0; \tag{3.3}$$

gas phase

$$\frac{\partial}{\partial x}(\rho u) + \frac{\partial}{\partial y}(\rho v) = 0, \tag{3.4}$$

$$\frac{\partial p}{\partial y} = 0, \quad \rho u \frac{\partial u}{\partial x} + \rho v \frac{\partial u}{\partial y} = -\frac{\partial p}{\partial x} + Pr \frac{\partial}{\partial y}\left(\mu \frac{\partial u}{\partial y}\right), \tag{3.5}$$

$$\rho u \frac{\partial T}{\partial x} + \rho v \frac{\partial T}{\partial y} - \frac{\partial^2 T}{\partial y^2} = q\omega, \tag{3.6}$$

$$\rho u \frac{\partial Y}{\partial x} + \rho v \frac{\partial Y}{\partial y} - L_F^{-1} \frac{\partial^2 Y}{\partial y^2} = -\omega, \tag{3.7}$$

$$\rho u \frac{\partial X}{\partial x} + \rho v \frac{\partial X}{\partial y} - L_X^{-1} \frac{\partial^2 X}{\partial y^2} = -\nu\omega, \tag{3.8}$$

$$\omega = D\rho^2 X Y \mathrm{e}^{-\mathscr{E}/T}, \quad \rho T = 1;$$

boundary conditions

$$\hat{u} = \hat{v} = 0, \quad \hat{T} = T_b \quad \text{at} \quad y = 0, \tag{3.9}$$

$$T = 1, \quad Y = 0, \quad X = X_\infty \quad \text{at} \quad y = H; \tag{3.10}$$

liquid–gas interfacial conditions, at $y = \varphi(x, t)$

$$m \equiv \rho\left(-u\frac{\partial \varphi}{\partial x} + v\right), \quad -\hat{u}\frac{\partial \varphi}{\partial x} + \hat{v} - \frac{\partial \varphi}{\partial t} = \alpha m, \tag{3.11}$$

$$u = 0, \tag{3.12}$$

$$\hat{p} - \alpha^2 p = -3S\frac{\partial^2 \varphi}{\partial x^2}, \tag{3.13}$$

$$-\frac{\partial \hat{u}}{\partial y} + \alpha^2\left(Pr\mu\frac{\partial u}{\partial y} + mu\right) = 2M\left(\frac{\partial \hat{T}}{\partial x} + \frac{\partial \varphi}{\partial x}\frac{\partial \hat{T}}{\partial y}\right), \tag{3.14}$$

$$\lambda^{-1}\frac{\partial \hat{T}}{\partial y} - \frac{\partial T}{\partial y} = -mL, \tag{3.15}$$

$$L_F^{-1}\frac{\partial Y}{\partial y} = m(Y-1), \quad L_X^{-1}\frac{\partial X}{\partial y} = mX, \tag{3.16}$$

$$Y = K\mathrm{e}^{-A/T}. \tag{3.17}$$

The scaling we have adopted yields, in the liquid phase, equations that are consistent with lubrication theory, and in the gas phase the boundary layer equations.

Several parameters appear in equations (3.1)–(3.17). The gas-phase Prandtl number Pr, which has been defined earlier, represents the ratio of viscous to thermal diffusivities. The fuel and oxidizer Lewis numbers,

$$L_F = \mathscr{D}_{\mathrm{th}}/\mathscr{D}_F, \quad L_X = \mathscr{D}_{\mathrm{th}}/\mathscr{D}_X,$$

represent the ratio of the thermal diffusivity of the mixture to the mass diffusivities of fuel or oxidizer, respectively. Although Lewis numbers are typically near one, small variations above or below one are known to have significant effects on combustion processes. Such variations could result either because of different mobility of the fuels considered or because of the existence of an abundant inert in the gas phase that could alter the average thermal diffusivity. Heavier fuels such as hydrocarbons, for example, have a larger value of L_F than alcohols and, the value of L_X could be reduced by diluting the ambient with CO_2, say, because of its larger heat capacity. The heat release parameter q, and the related parameter q' are given by

$$q = (Q/c_{p_g}T_\infty)(Y_\ell/\nu_F W_F), \quad q' = qX_\infty/\nu,$$

with $\nu = \nu_X W_X/\nu_F W_F$ the mass-weighted stoichiometric coefficient. In the parametric study presented below the parameter q' is found to be more useful; it represents the ratio of the energy liberated per unit mass of available oxidizer to the total energy in the ambient gas. The latent heat parameter L is given by $L = L_{\mathrm{v}}/c_{p_g}T_\infty$. The surface tension parameter and Marangoni number,

$$S = \sigma_0\rho_\ell h\epsilon^2/3\mu_\ell^2, \quad M = \gamma h T_\infty \rho_\ell/2\mu_\ell^2,$$

measure the level of surface tension and its gradient, respectively; they will be further discussed below. The reciprocal of the Froude number

$$G = \rho_\ell^2 h^3|\boldsymbol{g}|/\mu_\ell^2$$

measures the importance of gravity relative to inertia effects. The Damköhler number

$$D = \nu_F \rho_g Y_\ell h^2 \mathscr{B}/W_X \mathscr{D}_{\mathrm{th}}$$

is the ratio of the diffusion time to the chemical reaction time and is typically large suggesting that the chemical reaction rate is relatively fast. The activation energy parameter $\mathscr{E} = E/R^o T_\infty$ measures the sensitivity of the chemical reaction rate to temperature. Finally, the equilibrium coefficients

$$K = \frac{(P^o/P_\infty)\bar{W}}{Y_\ell W_F}\exp\left[\frac{L_{\mathrm{v}}}{R^o T_B/W_F}\right], \quad A = \frac{L_{\mathrm{v}}}{R^o T_\infty/W_F}$$

appear from scaling the Clausius–Clapeyron relation. With the exception of the Damköhler number D, all the parameters will be treated as $O(1)$ quantities.

4. Evolution equation

4.1. *The gas phase*

Although the mathematical formulation given above allows for a general external flow, we shall be concerned here with the special case in which the ambient gas is quiescent. This assumption, together with the requirement (3.12) imply that $u \equiv 0$ and, consequently, $p = 0$. The fuel vapour emanating from the surface of the film is transported everywhere vertically with a mass flow rate $m = \rho v$ that depends on the transverse coordinate and on time.

As noted earlier, the Damköhler number D is typically large. In the limit $D \to \infty$, known as the Burke–Schumann limit (Burke & Schumann 1928), the chemical reaction proceeds very fast so that fuel and oxidizer cannot co-exist. Complete combustion occurs along a reaction sheet, located at $y = y_f(x,t)$ say, where the fuel and oxidizer meet at stoichiometric proportions. This condition, which can be expressed as jump relationships across the sheet (cf. Cheatham & Matalon 2000)

$$[T]_{y_f^-}^{y_f^+} = [Y]_{y_f^-}^{y_f^+} = [X]_{y_f^-}^{y_f^+} = 0, \tag{4.1}$$

$$\frac{1}{q}\left[\frac{\partial T}{\partial y}\right]_{y_f^-}^{y_f^+} = -\frac{1}{L_F}\left[\frac{\partial Y}{\partial y}\right]_{y_f^-}^{y_f^+} = -\frac{1}{vL_X}\left[\frac{\partial X}{\partial y}\right]_{y_f^-}^{y_f^+}, \tag{4.2}$$

together with the requirements

$$Y|_{y_f^+} = 0, \quad X|_{y_f^-} = 0, \tag{4.3}$$

are sufficient to determine the combustion field as well as the instantaneous location of the reaction sheet. To this end one needs to solve the transport equations

$$m\frac{\partial T}{\partial y} - \frac{\partial^2 T}{\partial y^2} = 0,$$

$$m\frac{\partial Y}{\partial y} - L_F^{-1}\frac{\partial^2 Y}{\partial y^2} = 0, \qquad m\frac{\partial X}{\partial y} - L_X^{-1}\frac{\partial^2 X}{\partial y^2} = 0$$

on either side of the reaction sheet subject to (4.1)–(4.3) and the boundary conditions (3.10) and (3.16). One finds

$$Y = \begin{cases} 1 - \mathrm{e}^{-mL_F(y_f - y)}, & y < y_f \\ 0, & y > y_f, \end{cases}$$

$$X = \begin{cases} 0, & y < y_f \\ X_\infty \dfrac{\mathrm{e}^{mL_X(y-y_f)} - 1}{\mathrm{e}^{mL_X(H-y_f)} - 1}, & y > y_f, \end{cases}$$

$$T = \begin{cases} T_s + \left\{1 - T_s + q[\mathrm{e}^{m(H-y_f)} - 1]\right\} \dfrac{\mathrm{e}^{my} - \mathrm{e}^{m\varphi}}{\mathrm{e}^{mH} - \mathrm{e}^{m\varphi}}, & y < y_f \\ 1 + \left\{T_s - 1 + q[1 - \mathrm{e}^{-m(y_f - H)}]\right\} \dfrac{\mathrm{e}^{mH} - \mathrm{e}^{my}}{\mathrm{e}^{mH} - \mathrm{e}^{m\varphi}}, & y > y_f, \end{cases}$$

where T_s denotes the (surface) temperature at the interface that remains to be

determined. The location of the reaction sheet is given by

$$y_f = H - \frac{1}{m}\ln[(1+\nu^{-1}X_\infty)^{1/L_X}] \tag{4.4}$$

and the flame temperature T_f is obtained by evaluating T at $y = y_f$.

The only coupling between the liquid and gas phases remains in the mass and energy balances (3.11) and (3.15) and the Clausius–Clapeyron equation (3.17).

4.2. *The liquid phase*

The temperature in the film is easily obtained by integrating (3.3), leading to

$$T = T_b + (T_s - T_b)\frac{y}{\varphi}.$$

Integrating the momentum equations (3.2) and applying the conditions (3.9) and (3.13)–(3.14) one finds

$$\hat{p} = -3S\frac{\partial^2\varphi}{\partial x^2} + G(\varphi - y),$$

$$\hat{u} = E_1 y^2 + E_2 y, \quad \hat{v} = -\left(\frac{\partial E_1}{\partial x}\right)\frac{y^3}{3} - \left(\frac{\partial E_2}{\partial x}\right)\frac{y^2}{2},$$

where

$$E_1 = \frac{1}{2}G\frac{\partial\varphi}{\partial x} - \frac{3}{2}S\frac{\partial^3\varphi}{\partial x^3}, \quad E_2 = 3S\varphi\frac{\partial^3\varphi}{\partial x^3} - 2M\frac{\partial T_s}{\partial x} - G\varphi\frac{\partial\varphi}{\partial x}.$$

At this stage the velocity and pressure fields are completely determined in terms of the yet unknown function $\varphi(x,t)$.

4.3. *Interfacial conditions*

When the kinematic condition (3.11) is applied at the liquid–gas interface and use is made of the solutions in the gas and liquid phases, one finds

$$\frac{\partial\varphi}{\partial t} = -S\frac{\partial}{\partial x}\left(\varphi^3\frac{\partial^3\varphi}{\partial x^3}\right) + M\frac{\partial}{\partial x}\left(\frac{\partial T_s}{\partial x}\varphi^2\right) + \frac{1}{3}G\frac{\partial}{\partial x}\left(\varphi^3\frac{\partial\varphi}{\partial x}\right) - \alpha m \tag{4.5}$$

with m and T_s obtained from

$$m = \frac{L_F^{-1}}{H-\varphi}\ln\left\{\frac{(1+\nu^{-1}X_\infty)^{L_F/L_X}}{1-K\mathrm{e}^{-A/T_s}}\right\}, \tag{4.6}$$

$$\frac{1-T_s+q[(1+\nu^{-1}X_\infty)^{1/L_X}-1]}{\mathrm{e}^{m(H-\varphi)}-1} - \lambda^{-1}\frac{T_s-T_b}{m\varphi} = L, \tag{4.7}$$

which follow from applying conditions (3.15) and (3.17). The problem thus reduces to a single nonlinear partial differential equation (4.5) for the unknown $\varphi(x,t)$. It should be noted that equation (4.6) implies that T_s must satisfy the inequality $K\exp(-A/T_s) < 1$ which, in dimensional form, simply states that the surface temperature must be below the boiling temperature T_B.

5. Planar interface

The planar interface, which we shall denote here by $y = \eta(t)$ for convenience, recedes at a rate

$$\frac{\mathrm{d}\eta}{\mathrm{d}t} = -\alpha m \tag{5.1}$$

starting from the initial value $\eta(0) = 1$ to the disappearance of the film at $t = t_E$. Of primary interest is to determine the total evaporation time t_E, the surface temperature T_s, the evaporation or burning rate m and the flame standoff distance and temperature y_f and T_f, respectively.

5.1. *Isothermal film*

It is instructive to consider first the special case of an isothermal film. The temperature in the liquid is constant and remains equal to T_b at all times, so that $T_s = T_b$. This condition replaces the surface equilibrium condition (4.6) which must therefore be abandoned. Substituting in (4.7) and solving for m one obtains

$$m = \frac{\ln(1+B)}{H-\eta}, \tag{5.2}$$

where

$$B = \frac{1}{L}\{1 - T_b + q[(1+v^{-1}X_\infty)^{1/L_X} - 1]\} \tag{5.3}$$

is the conventional transfer number (Spalding 1952). The numerator of (5.3) consists of the difference in enthalpy between the ambient and the interface added to the heat released by the chemical reaction. Thus B is the ratio of the added energy which enhances the transfer to the latent heat of vaporization resisting the transfer. In the absence of combustion $B = (1 - T_b)/L$, which is the transfer number for the pure vaporization case. Equation (5.1), with m given by (5.2), can now be integrated to give

$$\eta = H - \sqrt{(H-1)^2 + 2\alpha \ln(1+B)t}$$

from which the total time for film evaporation can be deduced by setting $\eta = 0$, giving

$$t_E = \frac{2H-1}{2\alpha \ln(1+B)}. \tag{5.4}$$

Clearly $t_E > 0$ since $H > 1$. Furthermore, t_E increases with increasing L and decreasing q. By rewriting (5.4) in dimensional form it is readily seen that the characteristic evaporation time is indeed $\mathscr{D}_{\text{th}}^{-1}h^2(\rho_\ell/\rho_g)$, which is the unit of time we have chosen in scaling the equations divided by α. As noted earlier the factor α was introduced for convenience and has no particular physical meaning; it is used below as a scaling factor to enhance graph visualization. With m and B known, one obtains for the flame position and temperature

$$y_f = H - (H-\eta)\frac{\ln[(1+v^{-1}X_\infty)^{1/L_X}]}{\ln[1+B]} \tag{5.5}$$

and

$$T_f = T_b + L\left[\frac{1+B}{(1+v^{-1}X_\infty)^{1/L_X}} - 1\right]. \tag{5.6}$$

The flame temperature remains constant at all times. The flame position varies in time in a similar way as η; its initial position depends on the oxidizer concentration or mixture strength.

The results presented above are independent of the fuel Lewis number L_F which, as we shall see, is a consequence of the isothermal assumption. There is, however, an explicit dependence on the oxidizer Lewis number L_X; increasing L_X, for example by appropriately diluting the ambient gas, causes a decrease in B and therefore in the burning rate, thus extending the evaporation time t_E.

Since for an isothermal film all the heat available for evaporation is provided from the gas phase, an increase in the ambient temperature results in faster evaporation. Thus a decrease in T_b, the ratio of the film to the ambient temperature, causes an increase in B which produces a larger value of m and a shorter evaporation time t_E. Consistent with that we find that the flame temperature T_f decreases and the flame moves away from the film surface.

5.2. *Variable-temperature film*

When there is a variation in temperature throughout the film, the surface temperature T_s is an unknown that must be determined along with m and η from equations (4.6)–(4.7) and (5.1). We can write for the mass burning rate, similarly to (5.2), an expression of the form

$$m = \frac{\ln(1 + B_{\text{eff}})}{H - \eta}$$

except that now it depends on an 'effective transfer number' given by

$$B_{\text{eff}} = \frac{(1 + v^{-1}X_\infty)^{1/L_X}}{(1 - K\mathrm{e}^{-A/T_s})^{1/L_F}} - 1.$$

The surface temperature is determined from

$$\frac{1 - T_s + q[(1 + v^{-1}X_\infty)^{1/L_X} - 1]}{B_{\text{eff}}} - \lambda^{-1}\frac{T_s - T_b}{m\eta} = L.$$

As before B_{eff} represents the impetus to resistance of heat transfer, but because the resistance to the transfer depends on the local equilibrium, it is a function of time. For an isothermal film, obtained formally by taking the limit $\lambda \to \infty$, we see that B_{eff} reduces to the conventional transfer number B. Because of the transcendental nature of these relations, solutions are sought numerically. The results are shown in figures 2 and 3 where the dependence of η and T_s is plotted against time for different values of q' which, as noted earlier, is the more relevant parameter. The calculations reported are based on the following parameter values which are representative of alcohol and hydrocarbon fuels burning in air:

$$\left.\begin{array}{llll} \lambda = 0.2, & \mu = 2, & v^{-1}X_\infty = 0.067, & H = 6, \\ L = 1.3, & A = 20, & K = 6 \times 10^5, & T_b = 1.3, \\ L_F = 1, & L_X = 1, & Pr = 0.7. & \end{array}\right\} \tag{5.7}$$

Based on the value of μ and Pr, the factor $\alpha = 28.5$. The pure vaporization case is denoted by PV and has the longest evaporation time. The dependence of η on t, which is close to being linear for the pure vaporization case, becomes significantly nonlinear as q' increases.

For the pure vaporization case the surface of the film receives heat only from the hotter liquid below it. As the surface recedes, it heats up reaching T_b as $t \to t_E$. The surface temperature thus increases in time during the whole process. With sufficient combustion, however, this trend is reversed and the slope of T_s changes from positive to negative. The surface is now being heated mostly from above and cools off as it recedes, approaching T_b as $t \to t_E$. Since T_s can be significantly higher in this case, the evaporation time t_E is much shorter. The dependence of t_E on q' is shown in figure 4 along with the equivalent result for the case of an isothermal film. The evaporation times for the constant-temperature film are much smaller, as expected,

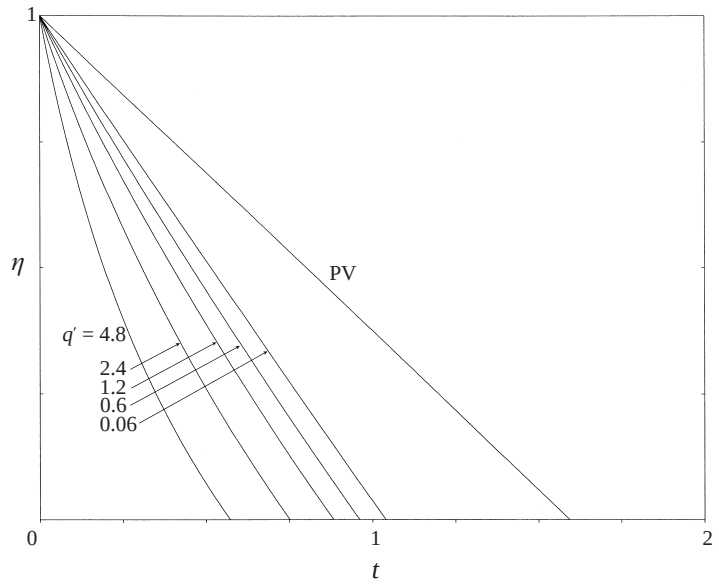

FIGURE 2. The position of the planar interface η as a function of time for various values of the heat release parameter q'. Here PV corresponds to the case of pure vaporization.

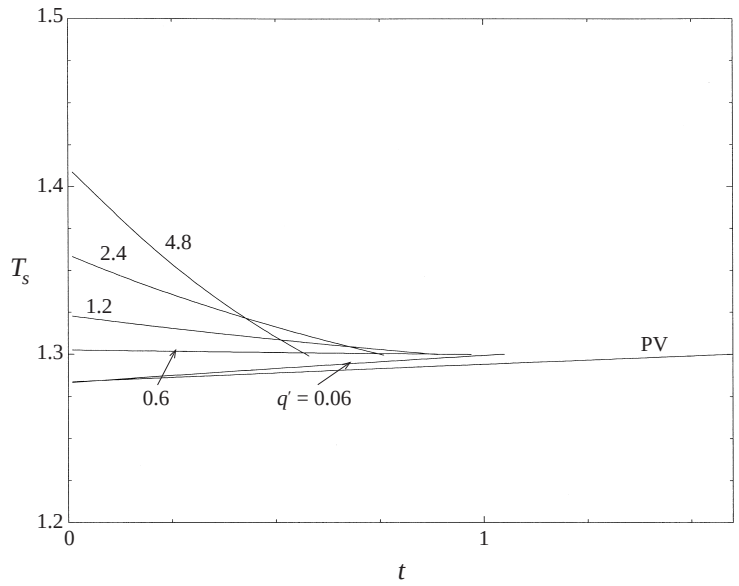

FIGURE 3. The surface temperature of the planar interface T_s as a function of time for various values of the heat release parameter q'. Here PV corresponds to the case of pure vaporization.

because by replacing the Clausius–Clapeyron equilibrium condition with a constant T_s, it is implied that the surface temperature is at or near the boiling temperature.

Unlike the constant-temperature case, the results here depend on both Lewis numbers L_F and L_X. It is found that as L_F increases, the flame moves closer to the film thereby increasing its surface temperature. The film, however, evaporates slower because of the decrease in the fuel–vapour mobility. Increasing L_X also causes

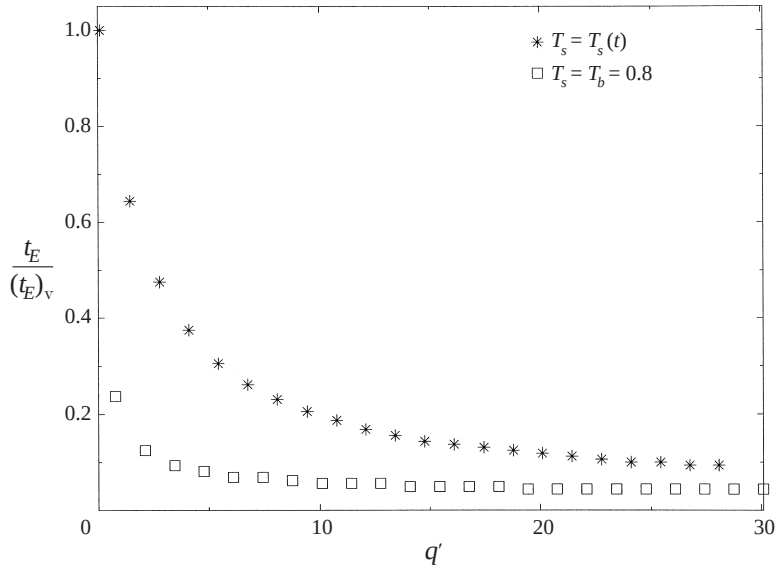

FIGURE 4. Evaporation time of a planar interface as a function of the heat release parameter q'. Time in the ordinate has been scaled with respect to the evaporation time for pure vaporization.

a slower evaporation of the film, as we found earlier. As a result of the reduced mobility of the oxidizer, the flame is located further away from the surface. This causes a reduction in heat flux to the surface and a slower evaporation process.

6. Spatially varying film

When the interface is no longer planar, gravity and surface tension play a significant role in the dynamics, as is evident from the evolution equation (4.5). In the following we shall consider in turn the response of the system to small disturbances, which permits linearizing the equation about the mean planar interface, and to finite disturbances where nonlinear effects become important.

6.1. *Linear stability*

We shall refer to the planar interface $y = \eta(t)$ discussed in the previous section as the basic state. At time $t = 0$ the surface of the film is slightly disturbed such that $\varphi(x, 0) = 1 + \psi_0 e^{ikx}$ with k the transverse wavenumber of the disturbance and ψ_0 its amplitude. The disturbance is first assumed small so that $|\psi_0| \ll 1$. We thus seek solutions of the form $\varphi(x, t) = \eta(t) + \psi(t)e^{ikx}$, substitute into equations (4.5)–(4.7) and linearize about the mean position, to obtain

$$\frac{1}{\psi}\frac{d\psi}{dt} = -[b_1(t)k^4 + b_2(t)k^2 + b_3(t)], \tag{6.1}$$

where

$$b_1 = S\eta^3,$$

$$b_2 = M\frac{H(\bar{T}_s - T_b)}{C_1 + C_2}\eta^2 + \tfrac{1}{3}G\eta^3,$$

$$b_3 = \alpha\left\{\frac{\ln(1 + B_{\text{eff}})}{(H - \eta)^2} + \delta\frac{H(\bar{T}_s - T_b)}{C_1 + C_2}\right\}.$$

Here $\bar{T}_s$ denotes the surface temperature of the basic state, and

$$\delta = \frac{L_F^{-1} AK \mathrm{e}^{-A/\bar{T}_s}}{\bar{T}_s^2 (1 - K\mathrm{e}^{-A/\bar{T}_s})},$$

$$C_1 = \frac{\lambda \eta^2 \ln(1 + B_{\mathrm{eff}})}{B_{\mathrm{eff}}} \left\{ 1 + \frac{\delta B_{\mathrm{eff}}}{1 + B_{\mathrm{eff}}} \left[1 + q(1 + v^{-1} X_\infty)^{1/L_X} - q - \bar{T}_s \right] \right\},$$

$$C_2 = \eta(H - \eta) \left\{ 1 - \delta \frac{\bar{T}_s - T_b}{\ln(1 + B_{\mathrm{eff}})} \right\}.$$

The basic state is considered stable, for a given k, if $\psi(t)$ is a monotonic decreasing function; it is considered unstable if $\psi(t)$ is a monotonic increasing function. In some instances, however, the amplitude of a disturbance starts decreasing, reaches a minimum value and then increases until the film's disappearance at $t = t_E$. In such a case we shall identify the state corresponding to $\mathrm{d}\psi/\mathrm{d}t = 0$ as the marginal state and the corresponding time, $t = t_*$, as the time of the onset of instability. Although this definition is somewhat arbitrary, because the disturbance may not grow in the remaining time to a sufficient size, it nevertheless represent the time when a significant change may occur in the film's evolution.

For an isothermal film, $\bar{T}_s = T_b$ and B_{eff} is replaced by the conventional transfer number B given by (5.3). The coefficients b_1, b_2, b_3 simplify significantly and equation (6.1) can be integrated exactly to yield

$$\psi(\eta) = \psi_0 \frac{H - 1}{H - \eta} \exp\left\{ -\alpha \frac{Sk^4 + \frac{1}{3} Gk^2}{\ln(1 + B)} \left[\frac{H}{4}(1 - \eta^4) - \tfrac{1}{5}(1 - \eta^5) \right] \right\}. \tag{6.2}$$

Since at all times, $\eta < 1$, we conclude that *all* disturbances decay in time. Hence, surface tension and gravity have a stabilizing influence on the evaporating film and any small disturbance of the surface decays in time. The absence of the Marangoni term is clearly a consequence of the constant surface temperature assumption.

For the general case, there are temperature variations along the film's interface and equation (6.1) cannot be simply integrated. Furthermore, since the coefficients b_i are time dependent, the range of the growing (unstable) modes changes in time. We will therefore identify the 'domain of instability' in the parameter space as the largest possible region of instability, namely conditions associated with the film becoming unstable at some time during the period $0 < t < t_E$. In order to determine the domain of instability we make use of the fact that the right-hand side of (6.1) is quadratic in k^2 and that the marginal states are the roots of this quadratic. Since $b_1 > 0$, the parabola is always concave down indicating that the unstable modes, at any given time, are limited to a finite range of wavenumbers. Unstable modes exist only when $b_2^2/4b_1 - b_3 > 0$. The range of wavenumbers is then limited to $k_-^2(t) < k^2 < k_+^2(t)$, where k_-^2 and k_+^2 are the two positive roots of the quadratic; when the smallest root is negative, we set $k_-^2 = 0$. For a given set of parameters the largest and smallest values of $k_\pm^2$, produced throughout the entire time interval $0 < t < t_E$, will be used to mark the boundary between stable and unstable states. The region of instability, therefore, represents the wavenumbers that are likely to grow at some time during the process, before complete evaporation occurs. The wavenumber corresponding to

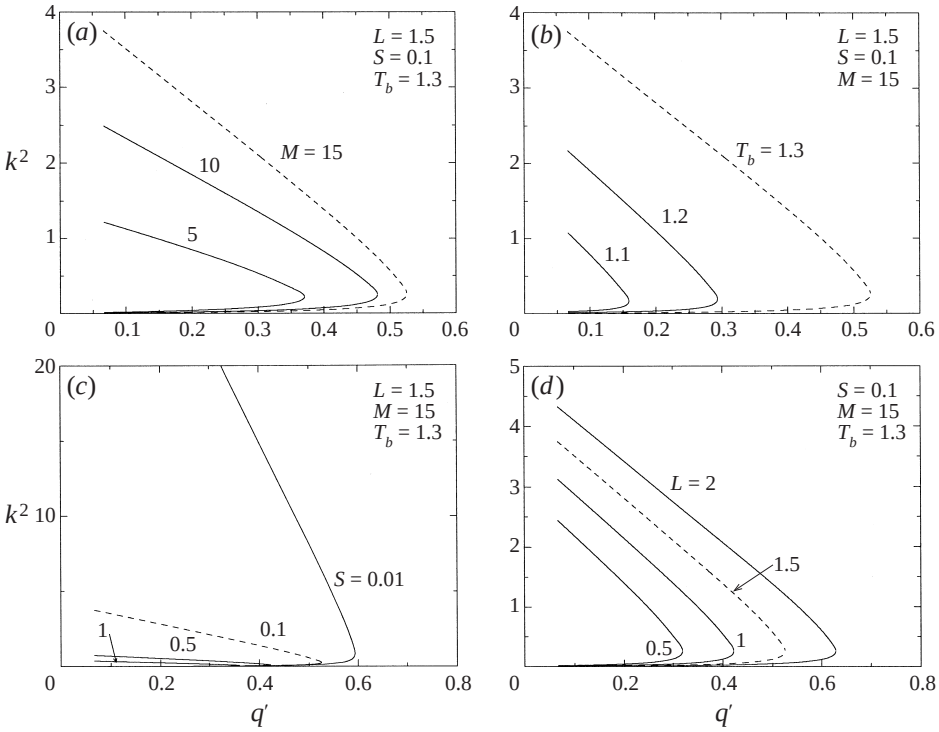

FIGURE 5. Neutral stability curves showing the dependence of the wavenumber k^2 on the heat release parameter q' in the absence of gravity ($G = 0$). Note that since the instability domain is changing in time what is being presented is the largest possible region of instability. The area to the left of the curves corresponds to unstable states. The dashed curves in each of the four graphs correspond to the same parameter values. We show the effect of varying: (*a*) the Marangoni number M, (*b*) the bottom temperature T_b, (*c*) the surface tension level S, and (*d*) the latent heat L.

the most rapidly growing mode is

$$k_{max} = \begin{cases} [-b_2/2b_1]^{1/2}, & b_2 < 0 \\ 0, & b_2 \geqslant 0. \end{cases} \tag{6.3}$$

In figure 5 we have plotted curves of marginal stability showing the range of unstable modes (those to the left of the curve) as a function of q' while varying one of the four other parameters: the surface tension S, the Marangoni number M, the ratio of the bottom of the film to the ambient temperatures T_b, and the latent heat L. This figure corresponds to the case $G = 0$, namely in the absence of gravity. Note that the dashed curves in each of the four plots represent the same curve. The results clearly indicate that the range of unstable modes is wider when M, L or T_b is increased, but is reduced when the level of surface tension S is increased. Heat release by combustion acts always as a stabilizing factor as is evident from all plots when q' is sufficiently large. The main mechanism for instability is clearly related to thermocapillary or Marangoni effects. Its destabilizing nature can be explained by examining the response of a small disturbance to an otherwise planar interface. Consider first the case of pure vaporization, namely $q' = 0$. A depression in the liquid–gas interface lies in a region that is hotter than its neighbours since $T_b > 1$. Since surface tension is a decreasing function of temperature (see equation

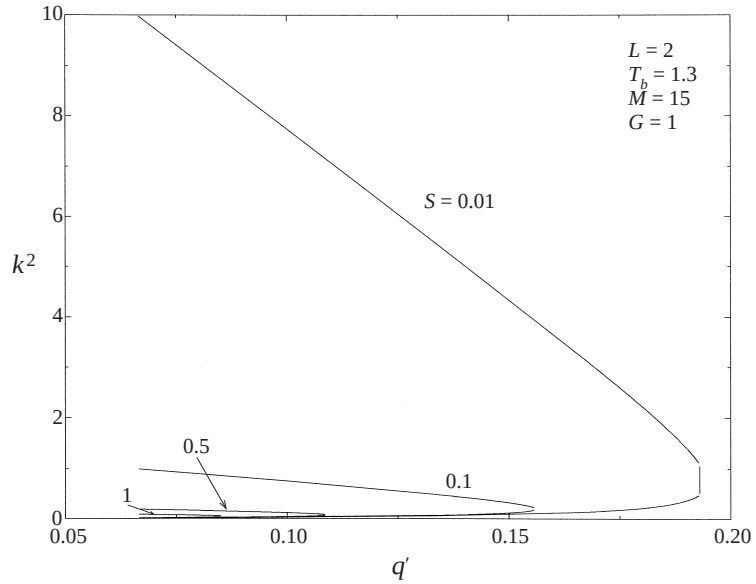

FIGURE 6. Neutral stability curves, similar to the one presented in figure 5(*d*), but in the presence of gravity ($G = 1$).

(2.21)) interfacial stresses drive liquid along the surface away from the depression and towards the crests. As the liquid near the surface is dragged along by viscous forces, the depression deepens further. Gravity and capillary forces cannot prevent this deepening and the film's thickness continues to decrease locally until it ruptures. In the presence of combustion the heat released in the gas phase is partially transported towards the interface. If the net heat flux at the interface is directed towards it, which would be the case when q' is sufficiently large, the intruding segments of the disturbed interface would lie in regions that are hotter than their neighbours. The flow of liquid near the interface is now directed towards the depressions, thus stabilizing the film. While heat release and thermocapillary effects are of primary importance in stabilizing/destabilizing the film, the role of the remaining parameters is to amplify or diminish these effects. Thus, for example, when T_b increases, the temperature difference between the depressed segments of the interface and their neighbours is also increased, thus enhancing the destabilizing mechanism. Similarly an increase in the latent heat L, which increases the resistance to heat transfer from the gas phase, reduces the stabilizing mechanism. Capillary forces, however, always act to stabilize the film.

As mentioned in the introduction Aharon & Shaw (1996) have examined the effects of thermocapillarity on the stability of an evaporating droplet. Although their results seem at first to contradict ours, a closer examination shows that this is not the case. In their configuration, the net flux of heat to the droplet's surface is always directed from the hot surrounding gas phase, a situation which is equivalent to ours when q is sufficiently large. Their conclusion, therefore, that Marangoni effects enhance stability is consistent with ours.

Figure 6 is similar to figure 5(*d*), except that now $G = 1$. Gravity here is the dominant effect and is clearly a stabilizing mechanism. Note that the critical q' for stability is reduced significantly compared to the case when $G = 0$.

6.2. *Nonlinear dynamics*

To examine the evolution of the interface resulting from a finite-amplitude disturbance, the nonlinear partial differential equation (4.5) has been solved numerically on a closed interval with periodic boundary conditions. The integration proceeds from an initial state, corresponding to the one that is likely to grow the fastest based on the linear stability results, until rupture. Rupture is defined when one point of the interface touches the bottom $y = 0$, and the 'rupture time' is the time it takes to reach that state. Fourth-order central differencing was used to compute the spatial derivatives. The time marching was accomplished by using the Netlib routine LSODA (Petzold & Hindmarsh 1987). This set of routines is a robust package which uses the information available at the end of each time step of the integration for making a decision as to which method to use and, accordingly, switches between stiff and non-stiff methods utilizing adaptive time steps to move forward or backward in time. In the worst case, for a very stiff system, the time marching is second order; but since at each time step the system is being re-evaluated, typically higher-order schemes are being used (Petzold 1983). A spatial grid refinement was used to determine the optimum number of grid points needed to obtain sufficiently smooth solutions. This was accomplished by increasing the number of grid points until the time to rupture no longer changed. In some cases an accurate rupture time could be found with a grid as low as $n = 40$, but it produced solutions which did not appear sufficiently smooth. With $n = 100$ the coarseness was significantly eliminated and the solutions were acceptable. However, due to the changing nature of k_{max}, the wavenumber associated with the fastest growing mode, a grid of $n = 100$ was not always sufficient to produce smooth curves. For example, coarse results were obtained at some instances when k_{max} was small. Because of this, the solutions depicted below utilize $n = 400$ ensuring smooth solutions with reliable rupture times for all values of k_{max} considered here.

The computations reported below use, for the most part, the parameter values listed in (5.7). A few exceptions were made in an attempt to demonstrate the different physical effects and to examine the interaction between various terms in the equation. We have fixed the domain of integration to ℓ so that $0 < x < \ell$, and considered periodic boundary conditions:

$$\varphi(0,t) = \varphi(\ell,t), \qquad \frac{\partial\varphi}{\partial x}(0,t) = \frac{\partial\varphi}{\partial x}(\ell,t),$$

$$\frac{\partial^2\varphi}{\partial x^2}(0,t) = \frac{\partial^2\varphi}{\partial x^2}(\ell,t), \quad \frac{\partial^3\varphi}{\partial x^3}(0,t) = \frac{\partial^3\varphi}{\partial x^3}(\ell,t).$$

In order to examine the solution over one wavelength, regardless of the value of the wavenumber k, we rescale the domain of integration by writing $x' = (2\pi/k)(x/\ell)$. Then $0 < x' < 2\pi/k$ and the parameters appearing in the evolution equation are modified to

$$S' = \frac{16\pi^4}{\ell^4}\frac{\sigma_0\rho_\ell h}{3\mu_\ell^2}\epsilon^2, \quad M' = \frac{4\pi^2}{\ell^2}\frac{\gamma T_\infty h\rho_\ell}{2\mu_\ell^2}, \quad G' = \frac{4\pi^2}{\ell^2}\frac{gh}{\mu_\ell^2/\rho_\ell^2 h^2}.$$

In the graphs reported below we have chosen $S' = 0.01, M' = 10$ and $G' = 0, 1$ or 5. The initial condition

$$\varphi(x,0) = 1 - 0.1\cos(k^o_{max}x) \tag{6.4}$$

was used, with k^o_{max} the maximizing wavenumber from linear theory at $t = 0$ (see equation (6.3)). The initial velocity and temperature profiles were taken to be the solutions corresponding to the choice of φ given in § 4.

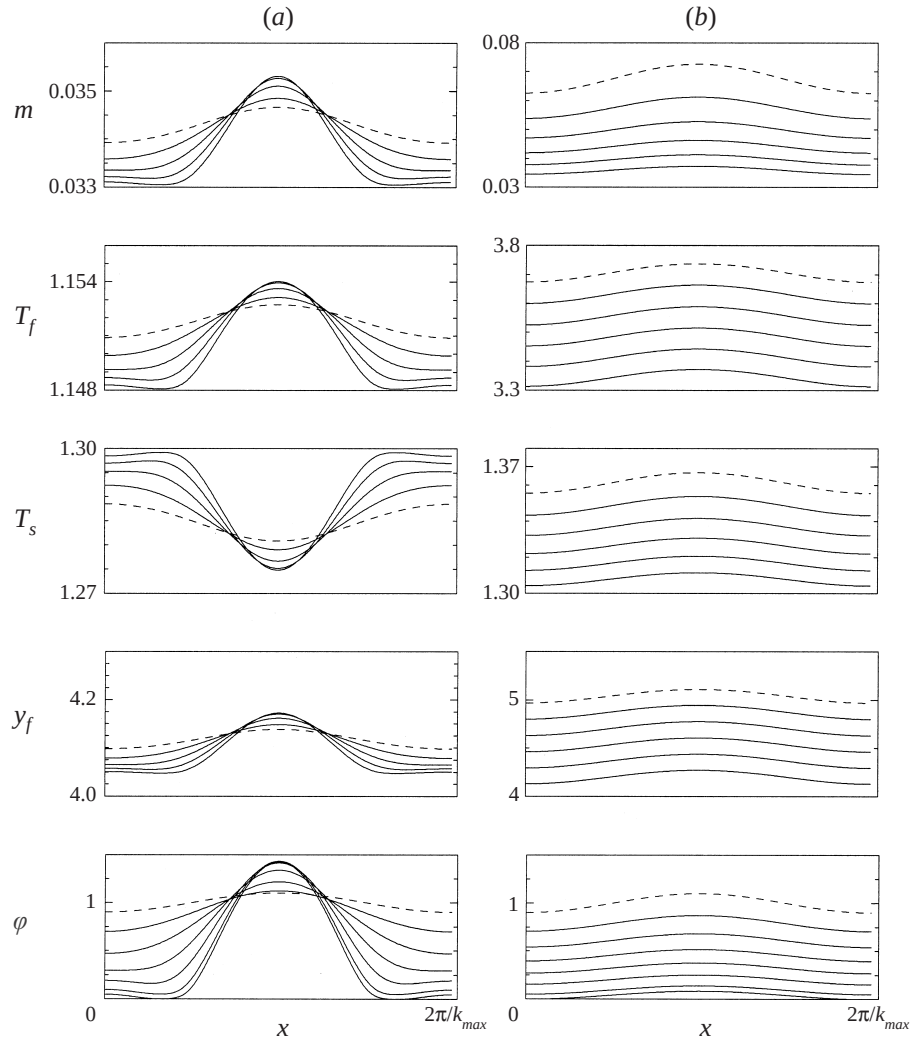

FIGURE 7. Profiles (from bottom to top) of film thickness, flame-sheet position, surface temperature, flame temperature and burning rate showing the spatial variations for consecutive times. The dashed curves in each case represents the initial profile. Graphs (*a*) correspond to an unstable case with $q' = 0.06$; (*b*) correspond to a stable case with $q' = 3$. Calculated for the parameter values used in (5.7) with $S' = 0.01$, $M' = 10$ and $G' = 0$.

The results are summarized in figures 7 and 9–11 where we have plotted over one period, from bottom to top, the shape of the interface φ, the flame position y_f, the surface temperature T_s, the flame temperature T_f and the mass burning rate m. The profiles are shown for consecutive times, for fixed intervals spanning the domain $0 \leqslant t < t_E$. The initial condition is denoted in all the figures by dashed curves.

Figure 7(*a*) corresponds to $q' = 0.06$ and illustrates the nonlinear development of an unstable basic state. In this case the film is heated from below ($T_b = 1.3$) and the ambient gas is relatively cold ($T_f \approx 1.15$). Although combustion is complete as a result of the assumed high Damköhler number, the diffusion flame is sitting far from the surface. It is located at $y_f \approx 4$ where the edge of the combustion layer is at $H = 6$. Thus, the surface of the film gains heat primarily from the hot liquid

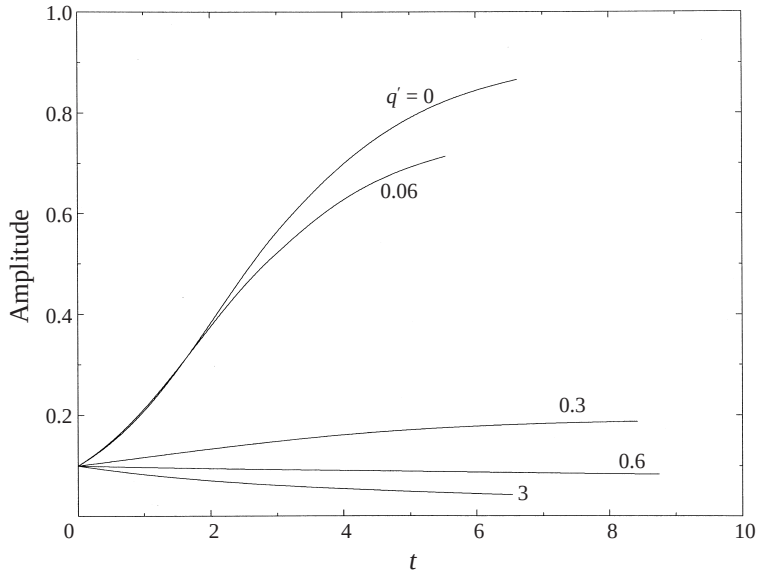

FIGURE 8. The dependence of the amplitude of the disturbed interface on time for various values of the heat release parameter q'. Calculated for the parameter values used in (5.7) with $S' = 0.01$, $M' = 10$ and $G' = 0$.

beneath it so that the surface temperature T_s is higher where the film is thinner and lower at the protruding sections. As discussed above, thermocapillary forces drive the liquid near the interface away from the depressed regions and towards the crests, thus feeding the growth of the initial perturbation. In contrast, a stable situation is illustrated in figure 7(*b*) corresponding to a moderate $q' = 3$. Here the flame temperature ($T_f \approx 3 - 4$) is higher than the surface temperature ($T_s \approx 1.3$) so that the film gains heat primarily from the gas above it. The surface temperature is thus higher at the crests and thermocapillary forces, which now drive the liquid near the interface towards the depressed regions, act to stabilize the film. The amplitude of the initial perturbation decays in time and the film becomes nearly planar as it continues to recede until $t = t_E$.

In figure 8 we show the time history of the amplitude of the film's interface for selected values of q' including the two values corresponding to figure 7. The amplitude at time t is defined as half the difference between the highest and lowest points of $\varphi(x, t)$. For $q' = 0.06$ the amplitude grows in time during the whole lifetime of the film, a situation which is clearly unstable. On increasing q' the rate of growth diminishes and for $q' = 0.6$ the amplitude decays for all time; a clearly stable configuration. We have also added in the figure a curve corresponding to the pure vaporization case ($q' = 0$) which is the most unstable scenario. Note that for a stable configuration, the ending time is approximately equal to the total evaporation time t_E of the basic state; it decreases with increasing q' as seen previously in figure 4. For an unstable configuration, however, the ending time appears to decrease with decreasing q'. This behaviour is attributed to the fact that, as the initial perturbation grows, the film ruptures first at one point and this occurs at a time $t < t_E$. The more unstable the interface is the shorter the time to rupture.

Figure 9 shows results corresponding to the same conditions as for the unstable situation depicted in figure 7(*a*) but in the presence of gravity. It is interesting to

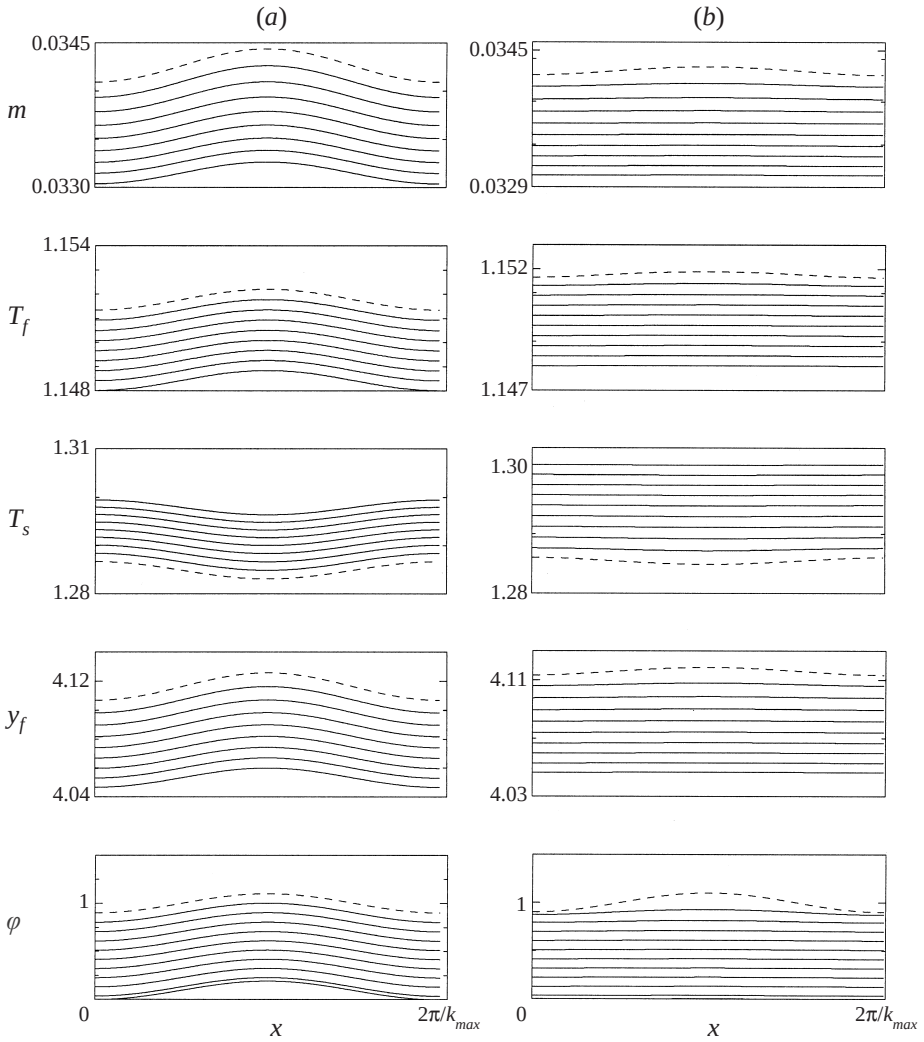

FIGURE 9. Similar to figure 7(*a*) with $q' = 0.06$, but in the presence of gravity: (*a*) corresponds to $G' = 1$ and (*b*) to $G' = 5$.

note that, although the surface temperature is higher at the depressed segments of the film and lowest at the crests, thermocapillary effects are not sufficient to promote instability; they are suppressed by gravitational forces. Although in both cases gravity is a dominant effect, the film never reaches a planar shape during the finite time interval $0 < t < t_E$ when $G' = 1$, unlike when $G' = 5$.

In figures 10 and 11 we show the effect of varying the Lewis numbers on the film dynamics, for unstable situations. Comparing the profiles in figure 10 we see that when $L_F < 1$, corresponding to a higher mass diffusivity of fuel, there is an increase in the mass loss from the film (increasing m) and consequently the flame stands further away from the film. Being closer to the ambient the flame temperature is lower, which explains the more unstable behaviour of the film in this case, compared to the case when $L_F > 1$ (see also figure 12). Comparing the profiles in figure 11 we see that, as a result of an increase in the oxidizer diffusivity, the flame stands closer to the film when $L_X < 1$ as opposed to when $L_X > 1$. Consequently the flame temperature is

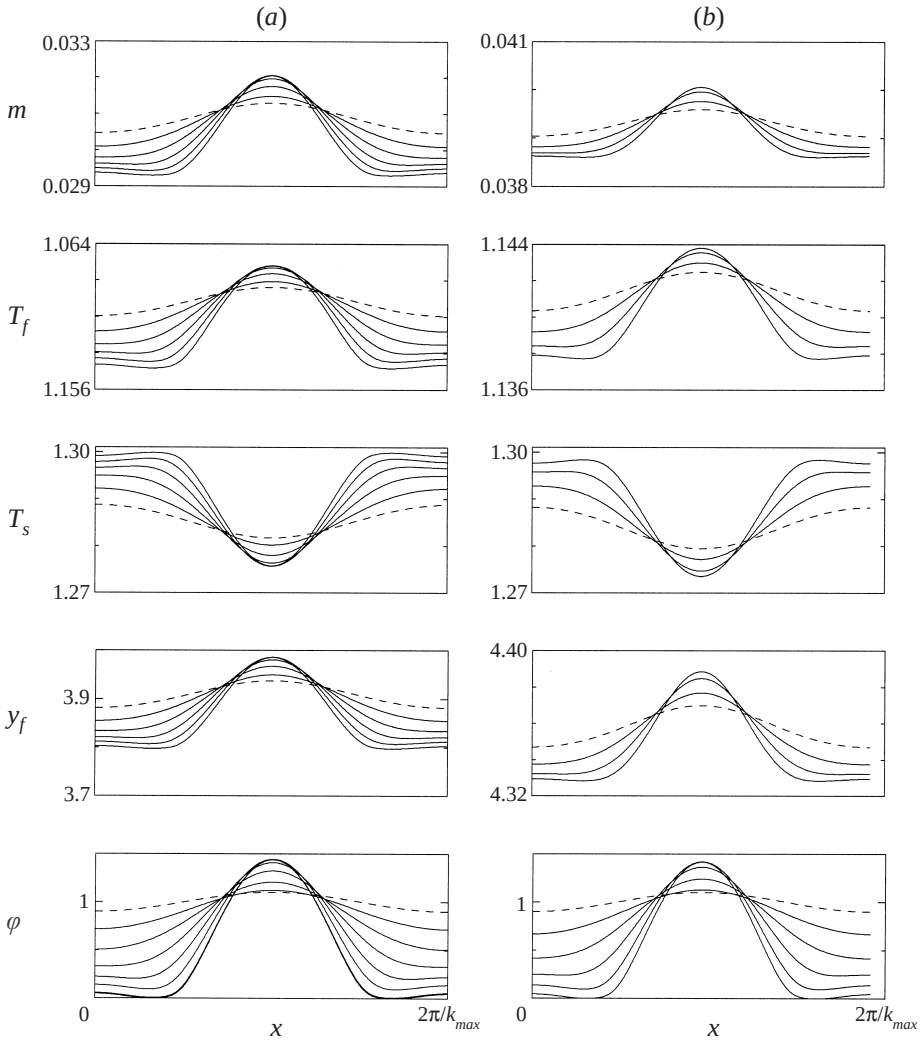

FIGURE 10. Similar to figure 7(*a*) with $q' = 0.06$, but with non-unity fuel Lewis numbers: (*a*) corresponds to $L_F = 1.2$ and (*b*) to $L_F = 0.8$.

higher and, since the surface of the film gains more heat from the gas phase, it is more stable (see also figure 12). Finally, one observes from figure 12 that despite the opposing trends regarding stability, increasing either L_F or L_X leads to an increase in the total evaporation time t_E.

7. Conclusions

In this work we are concerned with the evaporation and combustion of a thin film of liquid fuel. A long-wave approximation has been used to simplify the governing equations to what amounts to boundary layer equations in the gas phase and the lubrication approximation in the liquid phase. When the burning occurs in a quiescent ambient gas, the problem further reduces to an evolution equation for the film's thickness. What distinguishes this equation from previous studies of thin films is the additional two parameters that couple the dynamics of the film to the gas-phase

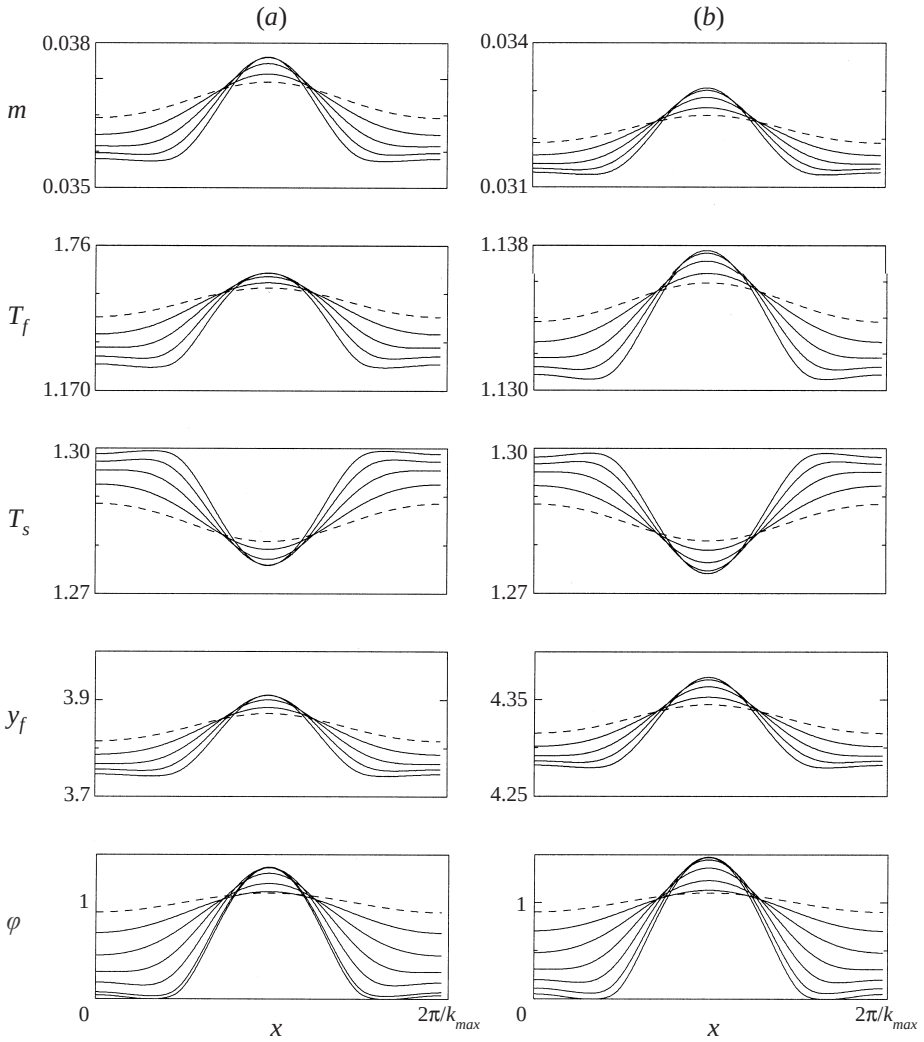

FIGURE 11. Similar to figure 7(*a*) with $q' = 0.06$, but with non-unity oxidizer Lewis numbers: (*a*) corresponds to $L_X = 0.8$ and (*b*) to $L_X = 1.2$.

processes. One of these parameters is the mass of fuel vapour leaving the surface of the film, which depends on the total heat conducted to the surface from both phases. The mass loss from the surface is closely related to the mass of fuel consumed at the diffusion flame which, in turn, depends on the ambient conditions as well as on the available oxidizer. The second parameter is the temperature at the surface of the film which depends on the local equilibrium conditions at the liquid–vapour interface.

In deriving the evolution equation (4.5) the viscosity of the liquid was assumed constant. Indeed, liquid viscosity varies substantially with temperature and, although it could have been possible to incorporate such a dependence in the analysis, we have ignored this effect for the sake of simplicity in order to focus our attention on the burning and its effect on the film's dynamics. A related study that accounts for variations in viscosity is that of Reisfeld & Bankoff (1990) who assumed a linear law, and considered the dynamics of a thin film without evaporation. They concluded

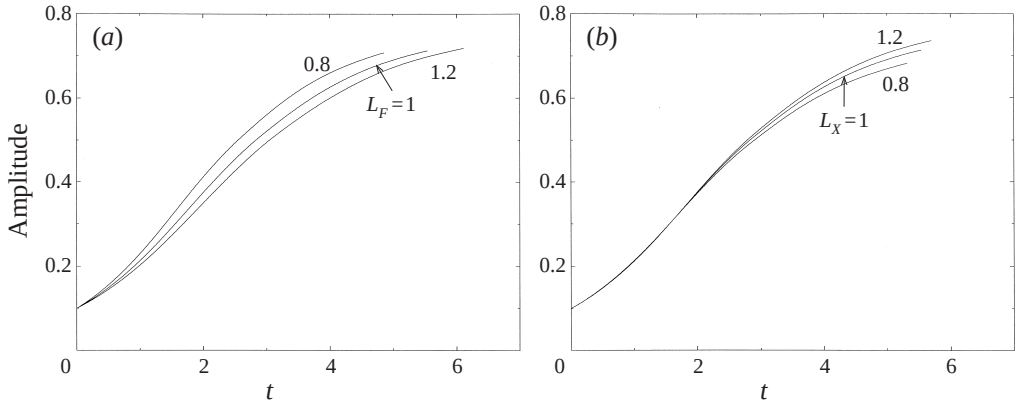

FIGURE 12. The growth of the amplitude: (*a*) variations of L_F for $L_X = 1$; (*b*) variations of L_X for $L_F = 1$.

that the effect of variable viscosity is just to reduce the time scale for the process, leading to a more rapid rupture of the film. However, the dependence of viscosity on temperature is more appropriately correlated by an exponential law which, being nonlinear, may have a more significant influence on the dynamics. Its effect, especially in the presence of evaporation and combustion, remains to be determined.

When the surface of the film remains planar the evolution equation describes the time rate of change of the film's thickness from its initial thickness until its disappearance. The liquid in this case remains stationary and there is only heat conduction across the liquid layer. Clearly combustion enhances the film's evaporation and disappearance. The results that include variables such as flame position and temperature, evaporation or burning rate, film thickness history and total evaporation time, exhibit an explicit dependence on the various physico-chemical parameters. Spatial non-uniformities in the initial conditions may grow or decay at a rate different from the rate at which the planar film recedes. We have thus examined the response to small disturbances, via a linear theory, and to finite-amplitude disturbances by numerically solving the nonlinear evolution equation. The main mechanism that drives the film toward or away from a planar state is thermocapillary effects. In the absence of combustion, or when the heat released is small, the surface of the film gains heat primarily from the liquid beneath it. Thermocapillary effects in this case drive the liquid near the surface in such a way as to cause the depression to deepen further and further. Gravity and capillary forces cannot prevent this deepening and the film's thickness continues to decrease locally until it ruptures. When the heat release by combustion is sufficiently high, the surface of the film gains heat primarily from the gas phase and thermocapillary forces act to stabilize the film. The role of all other parameters, such as the temperatures of the ambient and of the bottom of the film, the latent heat of vaporization, the oxidizer concentration in the ambient, the Lewis numbers, the level of surface tension and gravity, is to amplify or diminish the thermocapillary forces.

Our results have direct implications for microgravity combustion studies (King & Ross 1998), where the stabilizing effect of gravity is absent and surface tension effects become dominant. One such problem is the ignition and flame spread over liquid fuel beds (cf. Ross 1994). It is known that the thermocapillary or Marangoni effect is the driving mechanism for flame spread over fuels that are below the flash

temperature. For simplicity, the complex calculations of flame spread over liquid beds assume that the liquid–vapour interface is flat. Our stability results suggest that such an assumption can possibly be justified in the downstream region where the heat conducted back from the diffusion flame stabilizes any perturbation of the surface. However, near the leading edge, since the surface is primarily heated from below, surface deformation can be amplified and therefore must be accounted for. Indeed recent experimental work carried out at NASA Glenn shows that the surface deformation is quite significant and persists even in the trailing portion under the diffusion flame (H. O. Ross & F. J. Miller 2000, personal communication).

Finally, we note that there is a vast literature on convection resulting from the non-uniformity of surface tension along the free surface of a liquid layer heated from below. In such studies it has been recognized since the work of Scriven & Sternling (1964) that the deformation of the interface has a significant effect on the conditions for the onset of convection. Recent investigations by Hsieh & Pline (1991) and Skarda & McCaughan (1999), for example, have also explored the effect of surface deformation.

This work has been partially supported by the National Science Foundation under grants DMS 0072588 and CTS0074320 and by NASA's Microgravity Combustion Program. J. A. also acknowledges support from the Institute for Mathematics and its Applications, University of Minnesota. We are indebted to Dr Nimrod Sarig who carried out some of the preliminary linear stability calculations.

REFERENCES

Aharon, I. & Shaw, B. D. 1996 Marangoni instability of bi-component droplet gasification. *Phys. Fluids* **8**, 1820–1827.

Burelbach, J. P., Bankoff, B. G. & Davis, S. H. 1988 Nonlinear stability of evaporating/condensing liquid films. *J. Fluid Mech.* **195**, 463–494.

Burke, S. P. & Schumann, T. E. W. 1928 Diffusion flames. *Indust. Engng Chem.* **20**(10), 998–1004.

Cheatham, S. & Matalon, M. 2000 A general asymptotic theory of diffusion flames with application to cellular instability. *J. Fluid Mech.* **414**, 105–144.

Hsieh, K. C. & Pline, A. D. 1991 A comprehensive numerical study of surface tension driven convection with free surface deformation. *AIAA Paper* 91–1306.

King M. K. & Ross, H. D. 1998 Overview of the NASA microgravity combustion program. *AIAA J.* **36**(8), 101–118.

Krishnamoorthy, S., Ramaswamy, B. & Joo, S. W. 1995 Spontaneous rupture of thin liquid films due to thermocapillarity: A full-scale direct numerical simulation. *Phys. Fluids* **7**, 2291–2293.

Landau, L. D. & Lifshitz, E. M. 1959 *Fluid Mechanics*. Pergamon.

Oron, A., Davis, S. H. & Bankoff, S. G. 1997 Long-scale evolution of thin liquid films. *Rev. Mod. Phys.* **69**, 931–980.

Petzold, L. R. 1983 Automatic selection of methods for solving stiff and nonstiff systems of ordinary differential equations. *SIAM J. Sci. Statist. Comput.* **4**, 136–148.

Petzold, L. R. & Hindmarsh, A. C. 1987 LSODA. Computing and Mathematics Research Division, Lawrence Livermore National Laboratory, Livermore, CA.

Reisfeld, B. & Bankoff, S. G. 1990 Nonlinear stability of a heated thin liquid film with variable viscosity. *Phys. Fluids* A **2**, 2066–2067.

Ross, H. D. 1994 Ignition of and flame spread over laboratory-scale pools of pure liquid fuels. *Prog. Energy Combust. Sci.* **20**, 17–64.

Scriven, L. E. & Sternling, C. V. 1964 On cellular convection driven by surface tension gradients: Effects of mean surface tension and surface viscosity. *J. Fluid Mech.* **19**, 321–340.

Sirignano, W. A. & Glassman, I. 1970 Flame spreading above liquid fuels: surface-tension-driven flows. *Combust. Sci. Tech.* **1**, 307–312.

Skarda, J. R. L. & McCaughan, F. E. 1999 Exact solutions to stationary onset of convection due to surface tension variation in a multicomponent fluid layer with interfacial deformation. *Intl J. Heat Mass Transfer* **42**, 2387–2398.

Spalding, D. B. 1952 The combustion of liquid fuels. *Proc. Combust. Inst.* **4**, 847–864.

Williams, M. B. & Davis, S. H. 1982 Nonlinear theory of film rupture. *J. Colloid Interface Sci.* **90**, 220–228.